The Orthorhombic $(Ba_8Co_6O_{18})_\alpha(Ba_8Co_8O_{24})_\beta$ Series, a New Family of Monodimensional Oxides

K. Boulahya, M. Parras, and J. M. González-Calbet*

Departamento de Química Inorgánica, Facultad de Ciencias Químicas, Universidad Complutense, Madrid-28040, Spain

Received April 3, 2000. Revised Manuscript Received June 5, 2000

New forms of Ba−Co oxides with one-dimensional structures related to the 2H hexagonal perovskite have been synthesized and characterized by electron diffraction and high-resolution electron microscopy. All of them exhibit orthorhombic unit cells and can be considered as members of a new homologous series $(Ba_8Co_6O_{18})_\alpha(Ba_8Co_8O_{24})_\beta$. Their structures can be derived from the hcp stacking sequence of $Ba_8Co_2O_{18}$ and Ba_8O_{24} layers. Such a description allows very close structural relationships between this orthorhombic series and the rhombohedral $(Ba_3Co_2O_6)_\alpha(Ba_3Co_3O_9)_\beta$ family, also formed by a hcp stacking of mixed layers, but with different symmetry and stoichiometry, Ba_3CoO_6 and Ba_3O_9 layers. The ability of cobalt to be stabilized in all these different types of layers allows phases belonging to both rhombohedral and orthorhombic families to be isolated thus, leading to the presence of polymorphism, for some compositions.

Introduction

Polytypism is commonly used in solid-state chemistry to define different structures which can be regarded as built up by stacking layers with very close structure and composition and differ only in their stacking sequence. A typical example is shown for the 2H-ABO_3 hexagonal type whose structure is formed by isolated BO_6 octahedra running parallel to the *c*-axis as a consequence of the hexagonal packing of AO_3 layers where B cations occupy the octahedral sites defined by oxygen atoms.[1] When these layers are displaced ($^1/_3$ $^2/_3$) several hexagonal polytypes can be formed due to the introduction of cubic layers.[2] For instance, in the Ba−Co−O system, besides 2H-$BaCoO_3$,[3] 5H[4] and 12H[5] polytypes have been described.

In an interesting review of the different stoichiometries that can arise from a hexagonal packing of different layers, Darriet and Subramanian[6] have shown that the stacking of A_3O_9 and A_3BO_6 layers leads to a series of compounds which can be described as an ordered intergrowth between the 2H-$BaNiO_3$ [1] and Sr_4PtO_6 [7] structural fragments. The A−Co−O (A = Ba, Sr, Ca) system has became a singular candidate for the study of the mentioned phases since, from the careful selection of A cation, it has been possible to stabilize an exceptionally high number of compounds in the $(A_3Co_2O_6)_\alpha(A_3Co_3O_9)_\beta$ series.[8] All of them are formed by the ordered intergrowth of the two smallest structural units in the above formula and thus, could be considered as an example of recombination structures.[9] Both the chemical composition and the value of the *c*-parameter change as a function of the blocks the general structural features remaining constant. Their structures can be described as formed by infinite CoO_3 chains, running parallel to the *c*-axis, consisting of alternating octahedral and trigonal prismatic polyhedra separated by A cations. Many oxides showing these general features have been described in the past years,[10,11] and several approaches to determine their structures have been reported.[12,13]

Polymorphism is also present in the above A−Co−O system (A = Ba). Actually, by keeping Co in B positions it has been possible to prove the presence of polymorphism in the above family.[13] When the term $\alpha = 3$, $\beta = 5$, i.e., $Ba_8Co_7O_{21}$, is synthesized at 920 °C (5 days), a trigonal phase is stabilized.[14] The polyhedra rows constituting such a phase are formed by six octahedra and one trigonal prism sharing faces. The orthorhombic $Ba_8Co_7O_{21}$ phase,[15] obtained at lower temperature (875 °C, 6 days), keeps in every row the same polyhedra

* To whom correspondence should be addressed. Mailing address: José M. González-Calbet, Departamento de Química Inorgánica, Facultad de Químicas Universidad Complutense, 28040-Madrid, Spain. Telephone: 34 91 394 43 42. Fax: 34 91 394 43 52. E-mail: jgcalbet@eucmax.sim.ucm.es.

(1) Lander, J. *Acta Crystallogr.* **1951**, *4*, 148.
(2) Katz, L.; Ward, R. *Inorg. Chem.* **1963**, *3* (2), 205.
(3) Taguchi, H.; Takeda, Y.; Kanamara, F.; Shimada, M.; Kaizomi, M. *Acta Crystallogr. B* **1977**, *33*, 1299.
(4) Parras, M.; Varela, A.; Seehofer, H.; González-Calbet, J. M. *J. Solid State Chem.* **1995**, *120*, 327.
(5) Jacobson, A. J.; Hutchison, J. L. *J. Solid State Chem.* **1980**, *35*, 334.
(6) Darriet, J.; Subramanian, M. A. *J. Mater. Chem.* **1995**, *5* (4), 543.
(7) Randall, J. J.; Katz, L. *Acta Crystallogr.* **1959**, *12*, 519.
(8) Boulahya, K.; Parras, M.; González-Calbet, J. M. *Chem. Mater.* **2000**, *12*, 25.
(9) Lima-de-Faria, J.; Hellner, E.; Liebau, F.; Makovicky, E.; Parthè, E. *Acta Crystallogr.* **1990**, *A46*, 1.
(10) Blake, G. R.; Sloan, J.; Vente, J. F.; Battle, P. D. *Chem. Mater.* **1998**, *10*, 3536.
(11) Battle, P. D.; Blake, G. R.; Sloan, J.; Vente, J. F. *J. Solid State Chem.* **1998**, *136*, 103.
(12) Evain, M.; Boucher, F.; Gourdon, O.; Petricek, V.; Dusek, M.; Berdicka, P. *Chem. Mater.* **1998**, *10*, 3068.
(13) Zakhour-Nakl, M.; Claridge, J. B.; Darriet, J.; Weill, F.; zur Loye, H. C.; Pérz-Mato, J. M. *J. Am. Chem. Soc.* **2000**, *122*, 1618.
(14) Boulahya, K.; Parras, M.; González-Calbet, J. M. *J. Solid State Chem.* **1999**, *142*, 419.

10.1021/cm001056v CCC: $19.00 © 2000 American Chemical Society
Published on Web 08/09/2000

Table 1. Chemical Composition and Treatment Conditions of the Studied Materials

composition	T (°C)	t (days)
$Ba_8Co_7O_{21}$	875	6
$Ba_9Co_8O_{24}$	875	4
$Ba_{10}Co_9O_{27}$	870	3
$Ba_{11}Co_{10}O_{30}$	840	4
$Ba_{12}Co_{11}O_{33}$	800	3

sequence but the spatial arrangement between the rows is different. In fact, its structure is also formed by a hcp of mixed layers related to a hexagonal AO_3 layer, but both symmetry and composition are different. o-$Ba_8Co_7O_{21}$ is formed by the alternation of one Ba_8O_{24} and one $Ba_8Co_2O_{18}$ layer. The latter presents an orthorhombic symmetry with parameters $a = 2a_{2H}$ and $b = 2\sqrt{3}a_{2H}$. The stacking of these mixed layers generates the same Co environment found in the rhombohedral series but in a different arrangement.

This paper proves that polymorphism in $Ba_8Co_7O_{21}$ is not an isolated case in the Ba−Co−O system. Besides, our attempts to prepare and characterize new monodimensional orthorhombic phases have led to establishing a new homologous series, which can also be considered as recombination structures, of general formula $(Ba_8Co_6O_{18})_\alpha(Ba_8Co_8O_{24})_\beta$ closely related to the rhombohedral $(Ba_3Co_2O_6)_\alpha(Ba_3Co_3O_9)_\beta$ series. The structural characterization by means of selected area electron diffraction (SAED) and high-resolution electron microscopy (HREM) shows that some members of the former series are polymorphs of the latter family.

Experimental Section

Orthorhombic $Ba_9Co_8O_{24}$, $Ba_{10}Co_9O_{27}$, $Ba_{11}Co_{10}O_{30}$, and $Ba_{12}Co_{11}O_{33}$ materials were prepared by heating in air stoichiometric amounts of $BaCO_3$ and Co_3O_4 under the conditions listed in Table 1. The average cationic composition was determined by inductive coupling plasma. The local composition in every crystal was established by energy dispersive spectroscopy (EDS) on a JEOL electron microscope 2000FX equipped with an energy-dispersive system LINK AN10000. Results are consistent with the nominal compositions. The oxygen content was determined within $\pm 10^{-2}$ from the average oxidation state of cobalt analyzed by titration using Mohr's salt.

Powder X-ray diffraction (XRD) was carried out on a Philips X'Pert diffractometer using Cu Kα radiation. Selected area electron diffraction (SAED) was performed on a JEOL 2000FX electron microscope, fitted with a double tilting goniometer stage (±45°). High-resolution electron microscopy (HREM) was performed on a JEOL 4000EX electron microscope, fitted with a double tilting goniometer stage (±25°), by working at 400 kV. Samples were ultrasonically dispersed in *n*-butanol and transferred to carbon-coated copper grids. Image simulations were calculated using the MacTempas package.

Results and Discussion

Figure 1 shows the powder (XRD) patterns corresponding to o-$Ba_{10}Co_9O_{27}$ and o-$Ba_{12}Co_{11}O_{33}$. The XRD pattern corresponding to o-$Ba_8Co_7O_{21}$ has also been included for comparison, since all of them and those obtained for $Ba_9Co_8O_{24}$ and $Ba_{11}Co_{10}O_{30}$, show similar characteristics. As found in o-$Ba_8Co_7O_{21}$,[15] the most intense reflections can be assigned to a 2H-$BaCoO_3$ hexagonal cell, indicating that the hexagonal stacking sequence is maintained in all the samples. It is also worth mentioning that the *c* axis hexagonal subcell parameter is in all cases smaller than that corresponding to the 2H-$BaCoO_3$ phase. This decreasing is related to a stoichiometric ratio Co/Ba < 1 as a consequence of the stabilization of some Co in prismatic coordination. Together with the most intense diffraction maxima, the presence of low intensity reflections (marked with an asterisk) indicates that these materials can also present orthorhombic symmetry. SAED and HREM have been used to elucidate the structural features of each phase. Hereinafter, subindex 2H will be used to denote the 2H-ABO_3 type, and subindex o will stand for the orthorhombic cells.

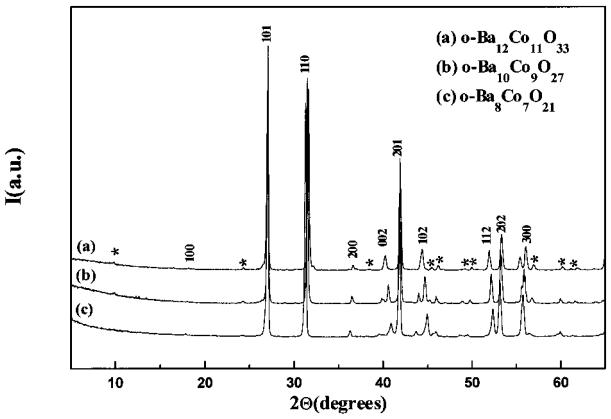

Figure 1. X-ray diffraction patterns corresponding to o-$Ba_{12}Co_{11}O_{33}$ (a), o-$Ba_{10}Co_9O_{27}$ (b), and o-$Ba_8Co_7O_{21}$ (c) materials.

Orthorhombic $Ba_{10}Co_9O_{27}$ and $Ba_{12}Co_{11}O_{33}$. SAED clearly shows that both materials present orthorhombic symmetry. As an example, we show in Figure 2 the most representative zone axes corresponding to o-$Ba_{10}Co_9O_{27}$. A 10-fold modulated superstructure along $[5\ 0\ \bar{5}\ 2]^*_{2H}$ and equivalent directions is seen along the $[1\ \bar{2}\ 1\ 0]_{2H}$ zone axis (Figure 2a). The $[1\ 1\ \bar{2}\ 0]_{2H}$ projection is identical. However, the reciprocal net along $[\bar{2}\ 1\ 1\ 0]_{2H}$ (Figure 2b) shows a 2-fold superlattice along $[0\ 1\ \bar{1}\ 0]^*_{2H}$ and a 5-fold superstructure along $[0\ 0\ 0\ 1]^*_{2H}$ and equivalent reflections where the most intense satellites are located at (0 0 *l*), $l = {}^1/_5, {}^4/_5$, and ($^1/_2$ 0 *l*), $l = {}^2/_5, {}^3/_5$.

Figure 2c shows the SAED pattern along $[1\ \bar{1}\ 0\ 0]_{2H}$. A 10-fold modulated superstructure along $[55i2]^*_{2H}$ is observed. The $[0\ 1\ \bar{1}\ 0]_{2H}$ projection (Figure 2d) shows a 2-fold superlattice along $[\bar{2}\ 1\ 1\ 0]^*_{2H}$ and another 10-fold superlattice along $[\bar{1}0\ 554]^*_{2H}$ axis is clearly seen. The $[1\ 0\ \bar{1}\ 0]_{2H}$ projection is identical to that shown in Figure 2c.

These patterns are in agreement with an orthorhombic symmetry and can be assigned on the basis of an orthorhombic unit cell with parameters $a = 1.14$ nm, $b = 1.98$ nm and $c = 2.25$ nm. According to this unit cell, the X-ray diffraction pattern is indexed as shown in Table 2.

Figure 3a shows the SAED pattern along $[1\ \bar{2}\ 1\ 0]_{2H}$ corresponding to o-$Ba_{12}Co_{11}O_{33}$. A 6-fold modulated superstructure is seen along $[3\ 0\ \bar{3}\ 1]^*_{2H}$ and equivalent directions. Along the $[\bar{2}\ 1\ 1\ 0]_{2H}$ projection (Figure 3b), satellite reflections are observed at (0 0 *l*) and (0 $^1/_2$ *l*) with $l = {}^1/_3$ and $^2/_3$, indicating the presence of a 2-fold superlattice along b^*_{2H} and a 3-fold superstructure along

(15) Boulahya, K.; Parras, M.; González-Calbet, J. M.; Vegas, A. *J. Solid State Chem.* **2000**, *151*, 77.

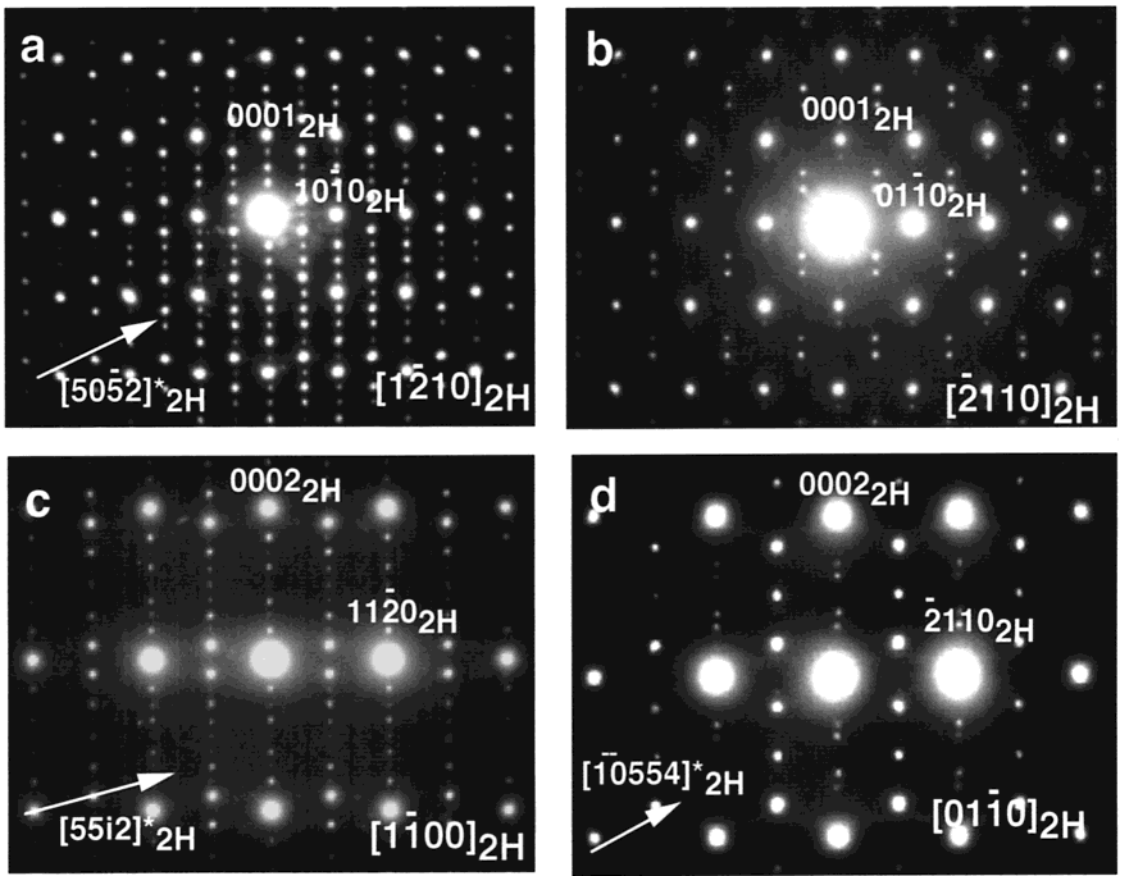

Figure 2. SAED patterns corresponding to o-$Ba_{10}Co_9O_{27}$ along the following zone axes: (a) $[1\ \bar{2}\ 1\ 0]_{2H}$, (b) $[\bar{2}\ 1\ 1\ 0]_{2H}$, (c) $[1\ \bar{1}\ 0\ 0]_{2H}$, and (d) $[0\ 1\ \bar{1}\ 0]_{2H}$.

Table 2. Powder X-ray Diffraction Data Corresponding to $Ba_{10}Co_9O_{27}$ and $Ba_{12}Co_{11}O_{33}$

$Ba_{10}Co_9O_{27}$				$Ba_{12}Co_{11}O_{33}$			
d_{obs} (nm)	d_{calc} (nm)	I/I_O	hkl	d_{obs} (nm)	d_{calc} (nm)	I/I_O	hkl
0.9005	0.9031	1.2	111	0.9148	0.9150	1.2	111
0.4969	0.4951	0.6	040	0.5457	0.5466	0.8	024
0.3682	0.3684	0.8	044	0.4945	0.4944	0.4	040
0.3296	0.3294	92	045	0.3318	0.3319	96	046
0.2857	0.2857	100	400	0.2853	0.2851	100	400
0.2475	0.2475	4.8	080	0.2470	0.2470	5.6	080
0.2206	0.2206	5.2	0010	0.2241	0.2241	6.2	0012
0.2158	0.2159	50.2	$08\bar{5}$	0.2164	0.2163	56.4	$08\bar{6}$
0.2070	0.2073	1	086	0.2059	0.2052	0.9	1610
0.2015	0.2015	9.8	$40\bar{1}0$	0.2041	0.2040	11.2	$40\bar{1}2$
0.1972	0.1972	3.9	$01\bar{0}1$	0.1975	0.1972	4.1	$80\bar{8}$
0.1870	0.1886	1.8	$0\bar{1}04$	0.1863	0.1859	1.8	0612
0.1841	0.1842	4.4	$0\bar{8}8$	0.1762	0.1768	10.7	$14\bar{1}4$
0.1747	0.1746	18	1312	0.1724	0.1727	18	$13\bar{1}5$
0.1722	0.1723	14	$08\bar{1}0$	0.1660	0.1656	9.1	$08\bar{1}2$
0.1648	0.1647	1.6	$01\bar{2}2$	0.1647	0.1647	16	$01\bar{2}0$
0.1550	0.1556	2.5	$0\bar{2}14$	0.1624	0.1619	2.8	$11\bar{2}2$
				0.1544	0.1546	1.6	$0\bar{1}\bar{2}6$

c^*_{2H}. All difraction maxima can be also indexed on the basis of an orthorhombic unit cell with the same *a*- and *b*-parameters as the previous $Ba_{10}Co_9O_{27}$ but with a different value of the *c*-parameter, $c = 2.7$ nm. All reflections appearing in the XRD pattern can be indexed on the basis of this unit cell (Table 2).

The ensemble of the above results indicate that both o-$Ba_{10}Co_9O_{27}$ and o-$Ba_{12}Co_{11}O_{33}$ present the same structural features that o-$Ba_8Co_7O_{21}$. Both the symmetry and the unit cell basis are identical and only differ in the *c*-parameter value. The SAED study shows that the *c*-axis in o-$Ba_{10}Co_9O_{27}$ is $c_o = 5c_{2H}$ while in o-$Ba_{12}Co_{11}O_{33}$ is $c_o = 6c_{2H}$ as a consequence of the different number of layers per unit cell. The o-$Ba_{10}Co_9O_{27}$ unit cell is formed by 10 layers, six Ba_8O_{24} and four $Ba_8Co_2O_{18}$, according to the chemical composition. For o-$Ba_{12}Co_{11}O_{33}$ the same reasoning leads to a unit cell constituted for eight Ba_8O_{24} and four $Ba_8Co_2O_{18}$ layers. The mixed stacking of such a layers originates, along *c*-axis, isolated rows of Co octahedrally and prismatically coordinated. For o-$Ba_8Co_7O_{21}$ material, these rows are formed by six octahedra and one trigonal prism (Figure 4a); therefore, the most simple structural models (Figure 4b,c) corresponding to both o-$Ba_{10}Co_9O_{27}$ and o-$Ba_{12}Co_{11}O_{33}$ incorporate one and two 2H structural blocks, respectively. If this is true, the layer sequence $4(Ba_8Co_2O_{18}/Ba_8O_{24})/2Ba_8O_{24}$ corresponds to o-$Ba_{10}Co_9O_{27}$ and the stacking sequence $[2(Ba_8Co_2O_{18}/Ba_8O_{24})/2Ba_8O_{24}]_2$ is the appropriate one for o-$Ba_{12}Co_{11}O_{33}$.

Having established that the SAED patterns of these materials are consistent with the basic structural principles outlined above, HREM has been used to prove the validity of these tentative structural models. Figure 5 shows the high-resolution image corresponding to o-$Ba_{10}Co_9O_{27}$ along $[1\ \bar{2}\ 10]_{2H}$. The thinnest area (marked A) only shows the ...ABAB... hexagonal packing of the 2H substructure. Simulated images at $\Delta t = 2.5$ nm and $\Delta f = -45$ nm nicely coincide with the experimental one. By increasing the thickness (zone B in the image) only equivalent layers are solved but the alternation of two white intense dots along *c* axis with three less intense dots is clearly appreciated. Such a contrast variation is also observed in the simulated image for $\Delta t = 5$ nm and

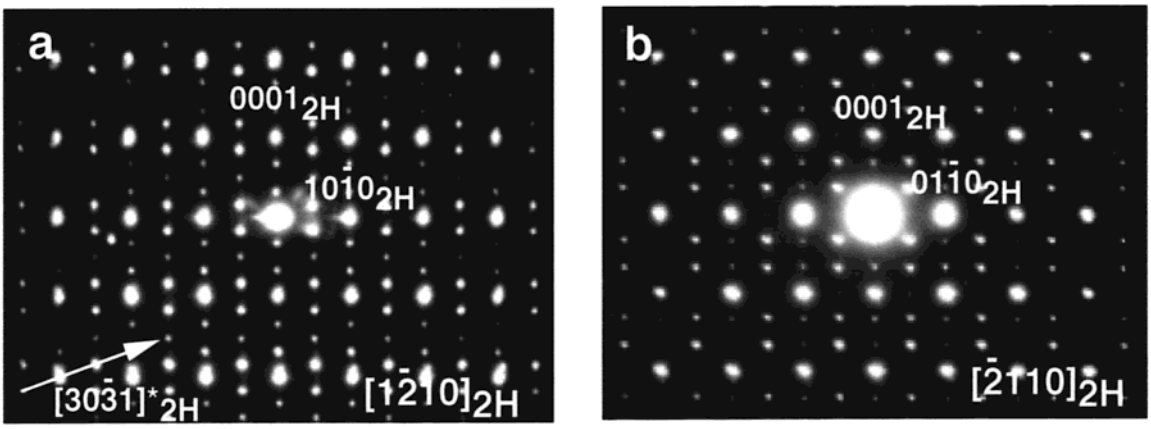

Figure 3. SAED patterns corresponding to o-$Ba_{12}Co_{11}O_{33}$ along $[1\,\bar{2}\,1\,0]_{2H}$ (a) and $[\bar{2}\,1\,1\,0]_{2H}$ (b) zone axis.

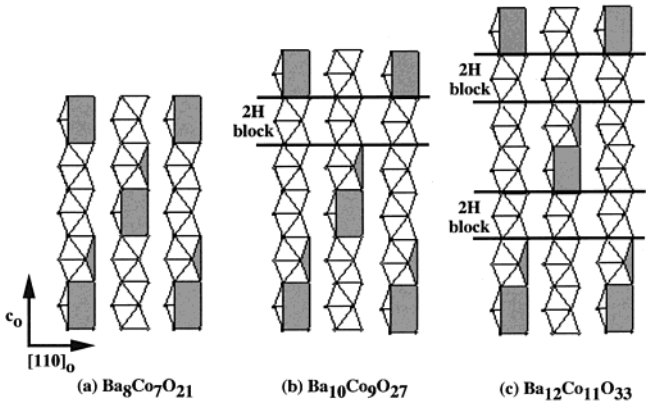

Figure 4. Schematic representation of the structural models proposed for o-$Ba_8Co_7O_{21}$, o-$Ba_{10}Co_9O_{27}$, and o-$Ba_{12}Co_{11}O_{33}$ viewed along the $[1\,\bar{2}\,1\,0]_{2H}$ direction.

Table 3. Chemical Composition and Crystallographyc Data of the Isolated Phases Belonging to the $(A_8B_6O_{18})_\alpha(A_8B_8O_{24})_\beta$ Series

composition	α	β	α/β	$\mathbf{k} = a^*_{2H}/2 + m\,2c^*_{2H}$ m
$A_4B_3O_9$	∞	0	∞	1/4
$Ba_8Co_7O_{21}$	1	1	1	1/8
$Ba_9Co_8O_{24}$	4	5	0.8	1/9
$Ba_{10}Co_9O_{27}$	2	3	0.67	1/10
$Ba_{11}Co_{10}O_{30}$	4	7	0.6	1/11
$Ba_{12}Co_{11}O_{33}$	1	2	0.5	1/12
$BaCoO_3$	0	∞	0	

$\Delta f = -30$ nm. The structural model along the same projection is inset in Figure 5. The overlaping of prisms and octahedra in consecutive rows perpendicular to the image plane leads to two positions ($z = 0$ and $^1/_5$) with similar electronic density. The environment of Co atoms at $z = {}^2/_5$, $^3/_5$, and $^4/_5$ is only octahedral giving a different contrast with respect to the previous one. By following the a_{2H} direction, the same contrast variation, displaced $^2/_5$ and $^3/_5$ along c, is observed as a consequence of the relative disposition of prisms and octahedra along such a direction.

The spatial arrangement of the polyhedra rows along the b_{2H} axis (b_o) can be seen in the HREM image shown in Figure 6a. Rows of intense dots alternate along c-axis with less intense dots according to a 1:(1):1:(2) sequence. Following the b_{2H} axis these rows are displaced $^1/_5c_o$. The same contrast variation is observed in the simulated image at $\Delta t = 4$ nm and $\Delta f = -35$ nm, in agreement with the structural model along such a projection depicted in Figure 6b. The overlaping of prisms and octahedra along the direction perpendicular to the image plane leads to two positions, $z = 0$ and $^2/_5$, with the same electronic density. For $z = {}^1/_5$, $^3/_5$, and $^4/_5$ only octahedral sites exist and the contrast is modified with respect to the previous one.

The HREM study of o-$Ba_{12}Co_{11}O_{33}$ shows the same experimental evidence. As an example, we show the structure image along $[1\,\bar{2}\,1\,0]_{2H}$ (Figure 7a). If we compare this image with that corresponding to o-$Ba_{10}Co_9O_{27}$ it can be observed that a new fringe of white dots appears (marked in Figure 7 with arrows). If we assign the contrast distribution in the same way as in the previous phase, this fringe can be associated with the insertion of two octahedra per polyhedra row, in agreement with the structural model depicted in Figure 7b. The calculated image at $\Delta t = 3.5$ nm and $\Delta f = -40$ nm fits with the experimental one.

These results confirm that the (10:9) phase can be derived from the (8:7) material by the addition of one frame of the 2H-$BaCoO_3$ phase, whereas the (12:11) structure is obtained by the introduction of two 2H-$BaCoO_3$ frames. This situation is analogous to that found in the monodimensional rhombohedral perovskite related compounds.[8] Actually, from the HREM results, all of the orthorhombic phases estabilized in the Ba−Co−O system can be considered as formed by the ordered intergrowth of the smallest units constituting their structures: $A_8B_8O_{24}$ (2H-ABO_3) and $A_8B_6O_{18}$ blocks, leading to the $(A_8B_6O_{18})_\alpha(A_8B_8O_{24})_\beta$ homologous series. The upper limit of this series would be the 2H-ABO_3 structural type ($\beta = \infty$) while the lower limit should correspond to an hypothetical term with the $A_4B_3O_9$ composition ($\alpha = \infty$), only constituted by $A_8B_2O_{18}$ orthorhombic layers. The α and β values of the three terms up to now described are gathered in Table 3.

All of the phases belonging to this family can be considered as modulated superstructures of the 2H-ABO_3 type. Effectively, a modulation is observed in all cases, but all reflections appearing in the SAED patterns, even those which can apparently be considered as satellites, can be indexed on the basis of conventional three-dimensional lattices. As a consequence, they can be described from the 2H basic unit cell with the modulation given by a vector $\boldsymbol{k}$, determined from the $[1\,\bar{2}\,1\,0]_{2H}$ zone, which can be expressed as $k = {}^1/_2\,a^*_{2H} + m\,2c^*_{2H}$, where m can be related to the number of the α and β blocks by means of the expression $m = \alpha/$

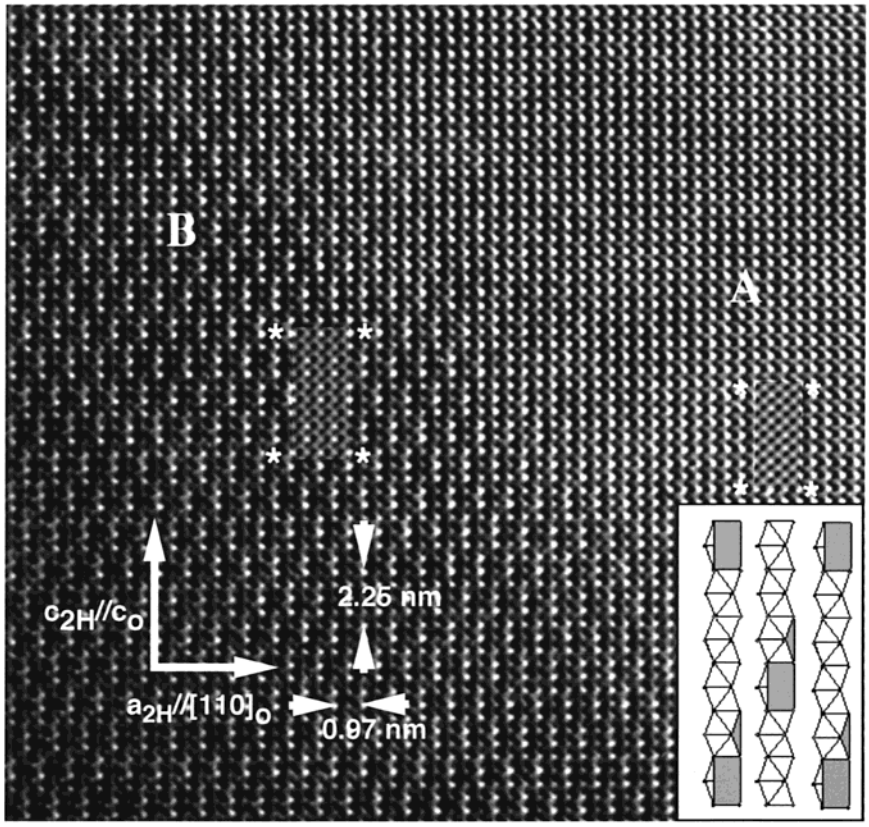

Figure 5. (a) HREM image of o-$Ba_{10}Co_9O_{27}$ along $[1\ \bar{2}\ 1\ 0]_{2H}$. Simulated images corresponding to zone ***A*** ($\Delta t = 2.5$ nm, $\Delta f = -45$ nm) and zone ***B*** ($\Delta t = 5$ nm, $\Delta f = -30$ nm) are at the inset. The structural model, depicted along the same projection, is also shown.

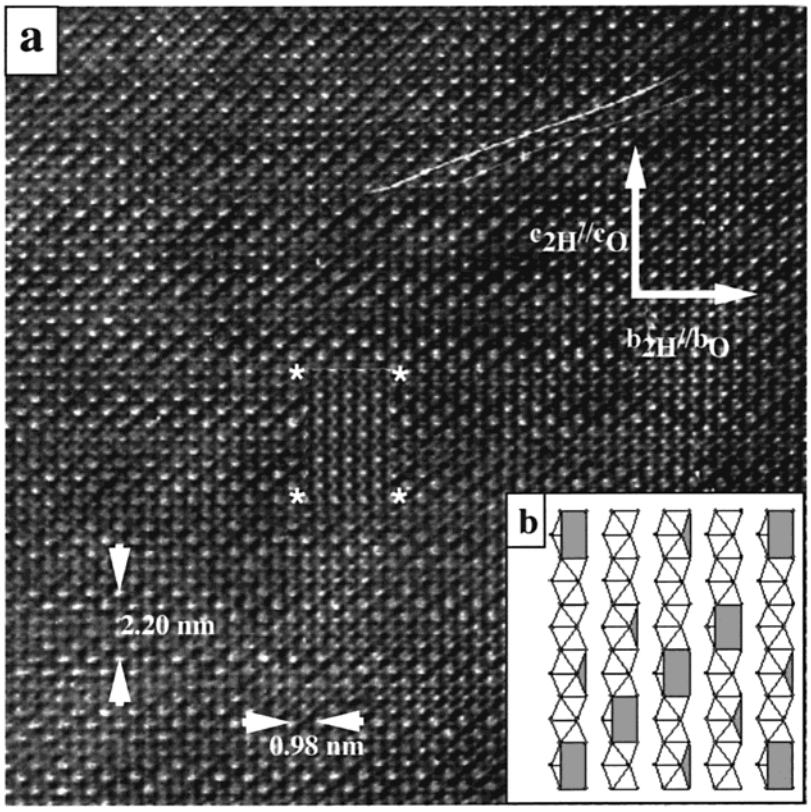

Figure 6. (a) HREM image of o-$Ba_{10}Co_9O_{27}$ along $[\bar{2}\ 1\ 1\ 0]_{2H}$. Simulated image is shown at the inset ($\Delta t = 4$ nm, $\Delta f = -35$ nm). (b) Schematic representation of the structural model along $[\bar{2}\ 1\ 1\ 0]_{2H}$.

$4(\alpha + \beta)$, with $[\alpha + \beta\ 0\ \mathrm{i}\ \alpha]^*_{2H}$ denoting the 2H superstructure direction. Such a direction corresponds to the perpendicular to the planes containing the Co atoms in trigonal prismatic coordination. The modulation

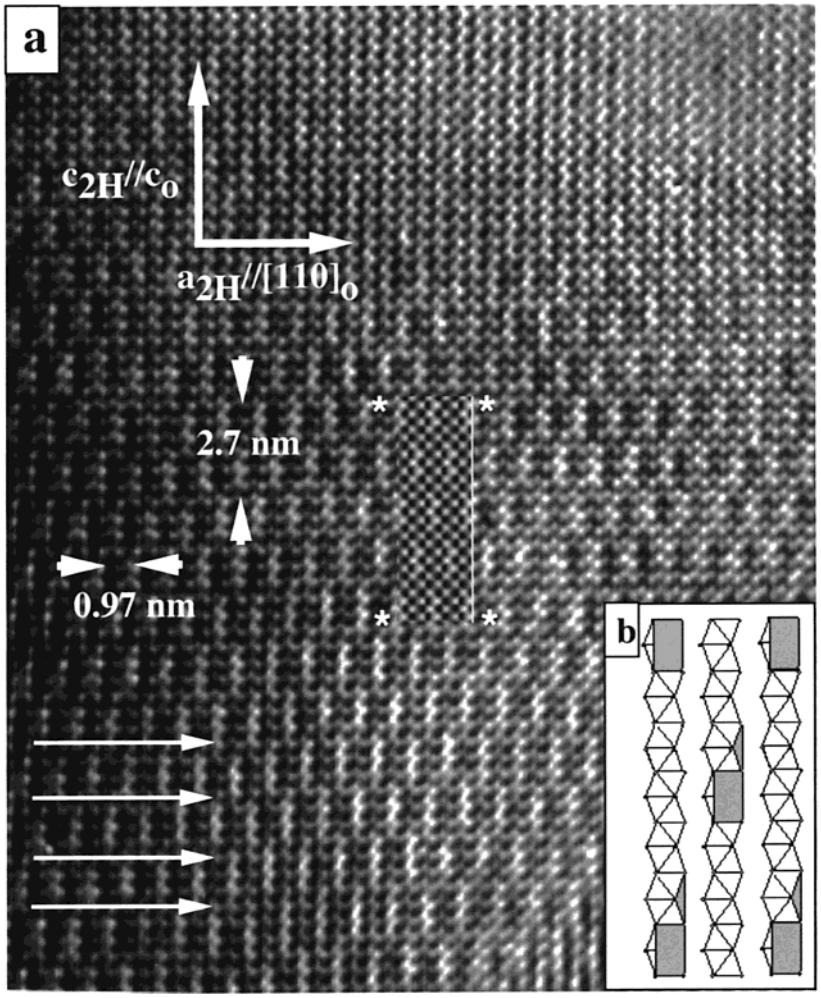

Figure 7. (a) HREM image of o-$Ba_{12}Co_{11}O_{33}$ along $[1\ \bar{2}\ 1\ 0]_{2H}$. The calculated image ($\Delta t = 3.5$ nm, $\Delta f = -40$ nm) is shown at the inset. (b) Corresponding structural projected along the $[1\ \bar{2}\ 1\ 0]_{2H}$ direction.

vector corresponding to every phase is also included in Table 3.

Orthorhombic o-$Ba_9Co_8O_{24}$ and o-$Ba_{11}Co_{10}O_{30}$. The chemical composition of the three terms previously described corresponds to nonconsecutive members of the above homologous series which have a common feature: the number of octahedra between trigonal prisms is constant for every phase. Intermediate terms have been synthesized for the composition $Ba_9Co_8O_{24}$ and $Ba_{11}Co_{10}O_{30}$. Their study by means of SAED and HREM reveals a slightly different structural situation.

Figure 8 shows the SAED pattern (a), the HREM (b), and the structure model (c) along $[1\ \bar{2}\ 1\ 0]_{2H}$ corresponding to $Ba_9Co_8O_{24}$. The 18-fold superlattice along $[9\ 0\ \bar{9}\ 4]^*_{2H}$ is defined by a vector $\boldsymbol{k} = {}^1/_2(a^*_{2H}) + {}^1/_9(2c^*_{2H})$. According to that, $\alpha = 4$, $\beta = 5$, i.e., 4 ($A_8B_6O_{18}$) blocks and 5 ($A_8B_8O_{24}$) blocks intergrow, per unit cell, along *c*-axis. This is in agreement with the contrast observed in the structure image (Figure 8b) where an ordered intergrowth between a unit cell of $Ba_8Co_7O_{21}$ and one of $Ba_{10}Co_9O_{27}$ is observed. Therefore, the $Ba_9Co_8O_{24}$ unit cell is constituted by 18 layers, 8 $Ba_8Co_2O_{18}$ and 10 Ba_8O_{24}, and the polyhedra sequence [1TP:$6O_h$][1TP:$8O_h$] results for every row as observed in the corresponding structural model (Figure 8c).

Figure 9 shows the SAED pattern (a), HREM (b), and structural model (c) along $[1\ \bar{2}\ 1\ 0]_{2H}$ corresponding to $Ba_{11}Co_{10}O_{30}$. In this case, a 22-fold modulated superlattice along $[1\ 1\ 0\ \overline{11}\ 4]^*_{2H}$ appears ($\boldsymbol{k} = {}^1/_2(a^*_{2H}) + {}^1/_{11}(2c^*_{2H})$). From this, the $\alpha = 4$, $\beta = 7$ values can be obtained, according to the corresponding HREM image where an ordered intergrowth between a unit cell of $Ba_{10}Co_9O_{27}$ and another $Ba_{12}Co_{11}O_{33}$ unit cell is observed. A total of 22 layers, 8 $Ba_8Co_2O_{18}$ and 14 Ba_8O_{24}, constitute the unit cell of the $Ba_{11}Co_{10}O_{33}$ phase, leading to a [1TP:$8O_h$][1TP:$10O_h$] polyhedra sequence in every row (Figure 9c).

These two new phases are also members of the orthorhombic $(A_8B_6O_{18})_\alpha(A_8B_8O_{24})_\beta$ homologous series (α and β values are also shown in Table 3). The only difference with respect to the other members is that the number of octahedra between trigonal prisms is not constant and they can be described as the ordered intergrowth between the upper and lower closest terms. In fact, if both $Ba_9Co_8O_{24}$ and $Ba_{11}Co_{10}O_{30}$ were formed by ...1TP:$7O_h$... and ...1TP:$9O_h$..., they should lead to the following ...ABAB... layer sequences: [4(A-$Ba_8Co_2O_{18}$/B-Ba_8O_{24})/A-Ba_8O_{24}]/B-$Ba_8Co_2O_{18}$... for $Ba_9Co_8O_{24}$ and [2(A-$Ba_8Co_2O_{18}$/B-Ba_8O_{24})/A-Ba_8O_{24}/B-Ba_8O_{24}/2(A-$Ba_8Co_2O_{18}$/B-Ba_8O_{24})/A-Ba_8O_{24}]/B-$Ba_8Co_2O_{18}$... for $Ba_{11}Co_{10}O_{30}$. The fact that these sequences are never obtained seems to indicate that the orthorhombic-$A_8B_2O_{18}$ layers must be equivalent.

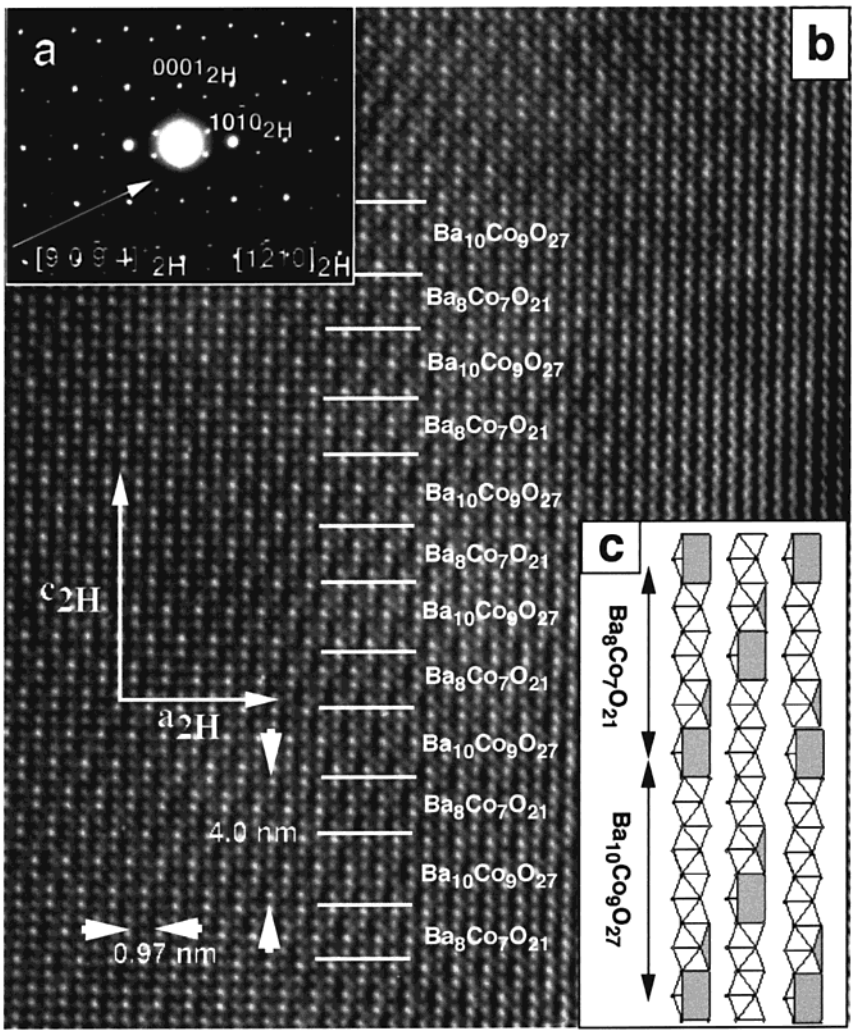

Figure 8. SAED pattern (a) HREM image (b) and structural model (c) along the $[1\ \bar{2}\ 1\ 0]_{2H}$ direction corresponding to o-$Ba_9Co_8O_{24}$ phase.

As it can be observed in Table 3, the member with a smaller Co/Ba ratio is o-$Ba_8Co_7O_{21}$, which is the lowest term up to now obtained in this series. However, the lower limit in the rhombohedral $(Ba_3Co_2O_6)_\alpha(Ba_3Co_3O_9)_\beta$ family is $Ca_3Co_2O_6$,[16] where only $A_3B_2O_6$ layers exist ($\alpha = \infty$, $\beta = 0$). According to that, it can be assumed that the lowest term of the orthorhombic series should also be formed by ∞ $A_8Co_2O_{18}$ layers, i.e., the $A_4Co_3O_9$ compound. Attempts to isolate materials with compositions such as $A_4Co_3O_9$ or $A_6Co_5O_{15}$ have not been successful up to now. In fact any term with a ratio $\alpha/\beta > 1$ should require that the orthorhombic $A_8Co_2O_{18}$ layers were not equivalent even when formed by the intergrowth of adjacent terms. For instance, the $\alpha = 4$, $\beta = 3$, corresponding to the $Ba_7Co_6O_{18}$ composition, should be formed by the intergrowth between $Ba_8Co_7O_{21}$ and $Ba_6Co_5O_{15}$. However, the latter requires the presence of $Ba_8Co_2O_{18}$ nonequivalent layers and, under the thermodynamics conditions we used, neither $Ba_7Co_6O_{18}$ nor $Ba_6Co_5O_{15}$ have been stabilized. This fact seems to confirm that only polytypes with structures formed by equivalent $Ba_8Co_2O_{18}$ layers can be stabilized, suggesting that $Ba_8Co_7O_{21}$ is, probably, the lowest term of this series. At this point, it is worth recalling that such kinds of structural limitations are also found in some metal transition sulfides.[17] FeS shows a NiAs structural type whose arrangement is equivalent to Ba−Co distribution in the 2H-$BaCoO_3$ structure. The formation of iron vacancies in the Fe−S system leads to orthorhombic phases up to Fe/S = $^7/_8$.[18] Besides, in the Cr−S system it has been observed that lower values than $^7/_8$ lead to trigonal or rhombohedral phases related to the NiAs structure.[19] Note, once again, that orthorhombic phases, in which the hcp stacking is maintained, can only be stabilized up to a limit which is governed by the existence of equivalent layers.

At this point, it is worth mentioning that all of the orthorhombic phases isolated in the Ba−Co−O system, could be grouped into a polysomatic series[20] by considering that the real lower term which it can be stabilized corresponds to o-$Ba_8Co_7O_{21}$. This one, together with 2H-ABO_3, constitutes the end-member structures. Both compounds, which present nearly identical two-dimensional structures, can be sliced into slabs that fit

(16) Fjellvag, H.; Gulbrandsen, E.; Aasland, S.; Olsen, A.; Hauback, B. C. *J. Solid State Chem*. **1996**, *124*, 190.

(17) Nakazawa, H. *Trans. Am. Crystallogr. Assoc.* **1979**, *15*, 107.

(18) Morimoto, N.; Gyobu, A.; Tsukuma, K.; Koto, K. *Am. Mineral.* **1975**, *60*, 240.

(19) Tilley, R. J. D. In *Crystallography and Crystal Chemistry of Materials with Layered Structures*; Levy, F., Ed.; D. Riedel Publishing Company: Boston, 1976; Vol. 2, p 127.

(20) Veblen, D. R. *Am. Mineral.* **1991**, *76*, 801.

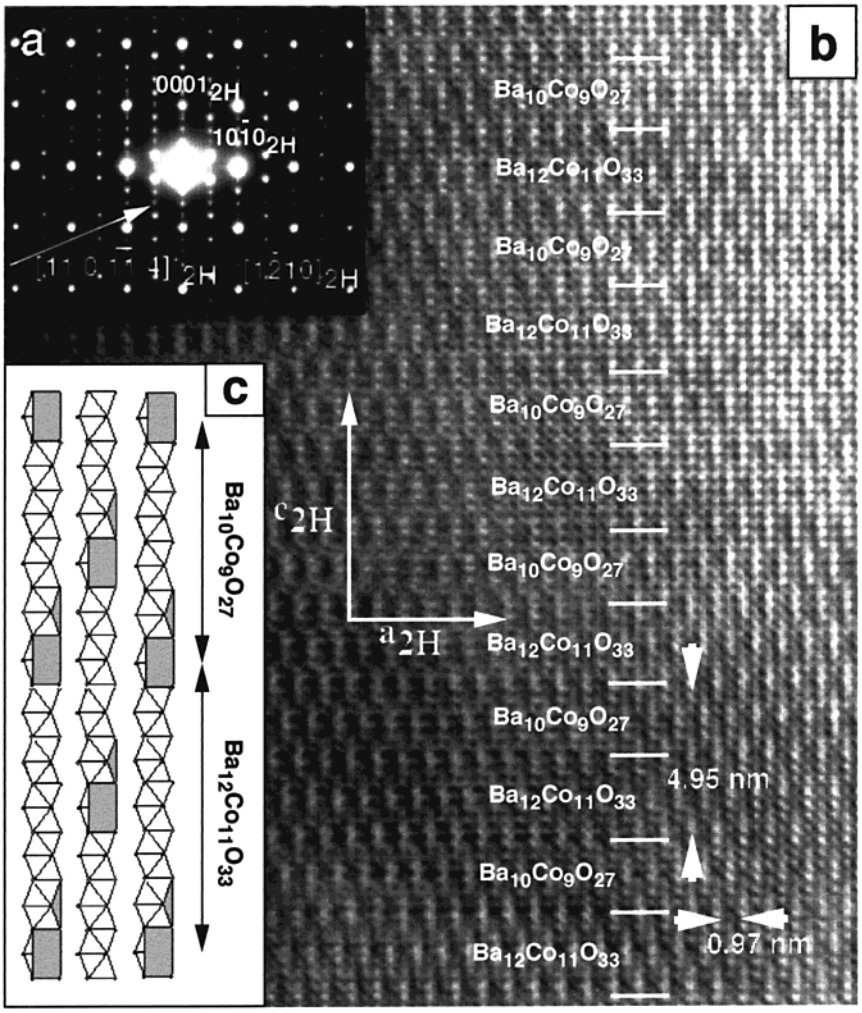

Figure 9. SAED pattern (a) HREM image (b) and structural model (c) along the $[1\ \bar{2}\ 1\ 0]_{2H}$ direction corresponding to o-$Ba_{11}Co_{10}O_{30}$ phase.

together almost perfectly. Actually, all of the stabilized orthorhombic phases, can be regarded as the ordered intergrowth between structural slabs of $^1/_2$ unit cell of the o-$Ba_8Co_7O_{21}$ phase (called *O*) and one $Ba_8Co_8O_{24}$ 2H-block (referred as *2H*), in different ratios, and, consequently, can be denoted as polysomatic structures. o-$Ba_9Co_8O_{24}$, $Ba_{10}Co_9O_{27}$, $Ba_{11}Co_{10}O_{30}$, and $Ba_{12}Co_{11}O_{33}$ are formed by mixing of the above-mentioned structural slabs in the following way: (*OOOO2H*), (*OO2H*), (*OO2HO2HO2H*), and (*O2H*), respectively, and these units are periodically repeated. Some of these polysomes are found to be polymorph with some members of the $(Ba_3Co_2O_6)_\alpha(Ba_3Co_3O_9)_\beta$ rhombohedral series. Besides o-$Ba_8Co_7O_{21}$, o-$Ba_9Co_8O_{24}$ has the corresponding polymorph in the former series with a special feature. The number of octahedra separating the trigonal prisms is not constant in the orthorhombic phase. In addition, the higher term up to now isolated in the rhombohedral series is $Ba_{66}Co_{59}O_{177}$ formed by the ordered intergrowth between $Ba_9Co_8O_{24}$ and $Ba_{10}Co_9O_{27}$. Although t-$Ba_{10}Co_9O_{24}$ has not been stabilized as a single phase, it can be considered as a polymorph of o-$Ba_{10}Co_9O_{24}$ with the same number of octahedra between trigonal prisms.

Concluding Remarks

All of the members of this new orthorhombic homologous series are gathered in Table 3, including α and β values for each one and the modulation vectors that describe these commensurate phases. It is worth mentioning that in all the phases, the modulation direction is perpendicular to the planes cointaining the Co atoms in a trigonal prismatic environment, as observed for the rhombohedral materials. This fact has been associated with the displacement of Co atoms in these sites in such a way that they are in off-centered positions along the trigonal axis.

The different members isolated in the Ba−Co−O system, $0 \le \alpha/\beta \le 1$, correspond, from a structural point of view, to solids with equivalent $Ba_8Co_2O_{18}$ layers. In this compositional range, different phases can be stabilized for any α and β values if adequate thermodynamic conditions are employed. However, such a stabilization seems not to be possible for $\alpha > \beta$. On the other hand, note that by assuming the II oxidation state for prismatically coordinated Co and the IV oxidation state for octahedrally coordinated Co, the charge balance is achieved whatever the α and β values. The chemical analysis only gives the average Co oxidation state, which, in all cases, fits with a ratio $Co^{II}(TP)/Co^{IV}(O_h)$, i.e., corresponding to $\alpha/(2\alpha + 4\beta) = Co^{II}/Co^{IV}$.

Alternatively, the SAED patterns can be indexed, as in the case of the rhombohedral series, using the composite crystal model considering the structures as formed by two subsystems.[21] The first one corresponds

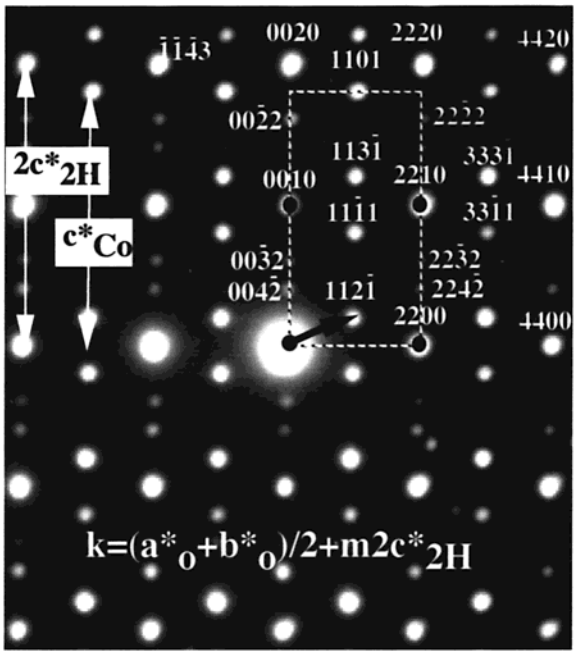

Figure 10. Indexation of the $[1\ \bar{2}\ 1\ 0]^*_{2H}$ plane, corresponding to o-$Ba_{10}Co_9O_{27}$, in a four-dimensional formalism to describe simultaneously the Ba and Co subsystems.

to the 2H-sublattice, a^*_{2H}, c^*_{2H} being the basic vectors of the reciprocal cell. The fundamental structure of the second subsystem, associated with the cobalt sublattice, has a orthorhombic lattice with $a^*_{Co} = a^*_{2H}/2$, $b^*_{Co} = 2(a^*_{2H} + b^*_{2H})/3$, and $c^*_{Co} = (1 - m)2c^*_{2H}$. The choice of a^*_{Co}, b^*_{Co}, c^*_{2H}, and c^*_{Co} as reciprocal vectors, allows one to describe simultaneously both sublattices with a set of four indices h, k, l, and m. For instance, Figure 10 shows the SAED pattern along $[1\ \bar{2}\ 1\ 0]$ corresponding to o-$Ba_{10}Co_9O_{27}$ phase, indexing on the basis of this fourdimensional description. ($hkl0$) and ($hk0m$) are the main reflections, while the less intense spots correspond to the satellite reflections originated by the interaction of the two subsystems. In the present case, the unit vector corresponding to the orthorhombic subsystem is given by $\boldsymbol{k} = (a^*_{Co}+b^*_{Co})/2 + {}^1/_{10}c^*_{2H}$.

In all the phases reported in this paper the c^*_{Co}/c^*_{2H} relationship corresponds to a rational fraction, i.e., to commensurate modulated structures and thus, they can be correctly described as modulated superstructures of the 2H-ABO_3 type. Obviously, such a description leads to very large unit cells, as 3.95 nm^3 for the smaller one which corresponds to $Ba_8Co_7O_{21}$ phase. As has been recently pointed out,[13] any attempts to solve the structure details for unit cells which such large volume, should lead to inaccurate results. However, SAED and HREM provide a useful tool to establish both, the building blocks constituting the structures (α and β values) and its stacking sequence, that is, the polyhedra sequence in every row and the spatial arrengement between them, thus leading to the essential structural features of each phase. From these results we have shown the existence of a new series in the Ba−Co−O system, which constitutes an example of polysomatism, where polymorphism between some phases belonging to this family and to the previously reported rhombohedral series is observed.

CM001056V

(21) Ukei, A.; Yamamoto, A.; Watanabe, Y.; Shishido, T.; Fukuda, T. *Acta Crystallogr. B* **1993**, *49*, 67.